Supplementary Figure 1

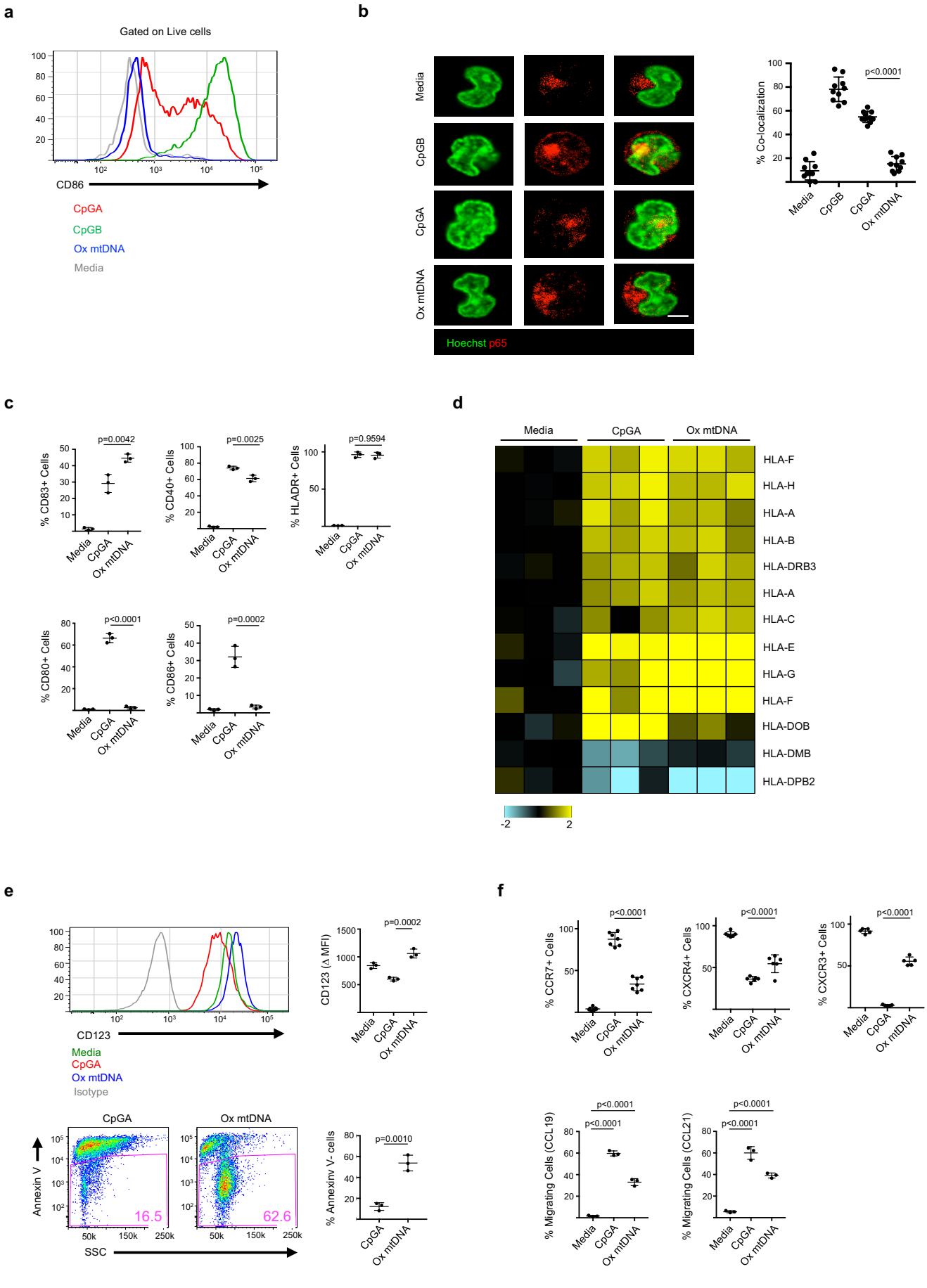

Supplementary Figure 1 | Ox mtDNA induces a unique pDC phenotype. a, Representative flow cytometry histogram of CD86 surface levels on pDCs activated for 24 h with CpGB, CpGA or Ox mtDNA. This experiment was repeated four times with similar results. **b,** Immunoflourescence analysis of p65 nuclear translocation in pDCs treated with CpGB, CpGA or Ox mtDNA. The % of p65 co-localizing with Hoechst is also shown (n=10 cells analyzed). This experiment was repeated three times with similar results. Scale bar = 7 μm. **c,** Percentage of $CD83^+$, $CD40^+$, $HLADR^+$, $CD80^+$ or $CD86^+$ pDCs in response to medium, CpGA or Ox mtDNA (n=3 independent experiments). **d,** Gene expression profile of HLA-related molecules in pDCs activated for 24 h with CpGA or Ox mtDNA (n=3 independent experiments). **e,** Upper panel: representative flow cytometry histogram of CD123 surface levels in pDCs activated for 24 h with CpGB, CpGA or Ox mtDNA (n=3 independent experiments). Lower panel: annexin-V staining of pDCs activated for 18 h with CpGA or Ox mtDNA and then rested for additional 24 h in the presence of IL3 (n=3 independent experiments). **f,** Upper panel: percentage of $CCR7^+$, $CXCR4^+$ and $CXCR3^+$ pDCs in response to medium, CpGA or Ox mtDNA (n=7 independent experiments). Lower panel: Migration assay of medium, CpGA or Ox mtDNA-activated pDCs toward the CCR7 ligands CCL19 and CCL21 (n=3 independent experiments). Shown are mean ± s.e.m.; statistical analysis by nonparametric one-way ANOVA.

Supplementary Figure 2

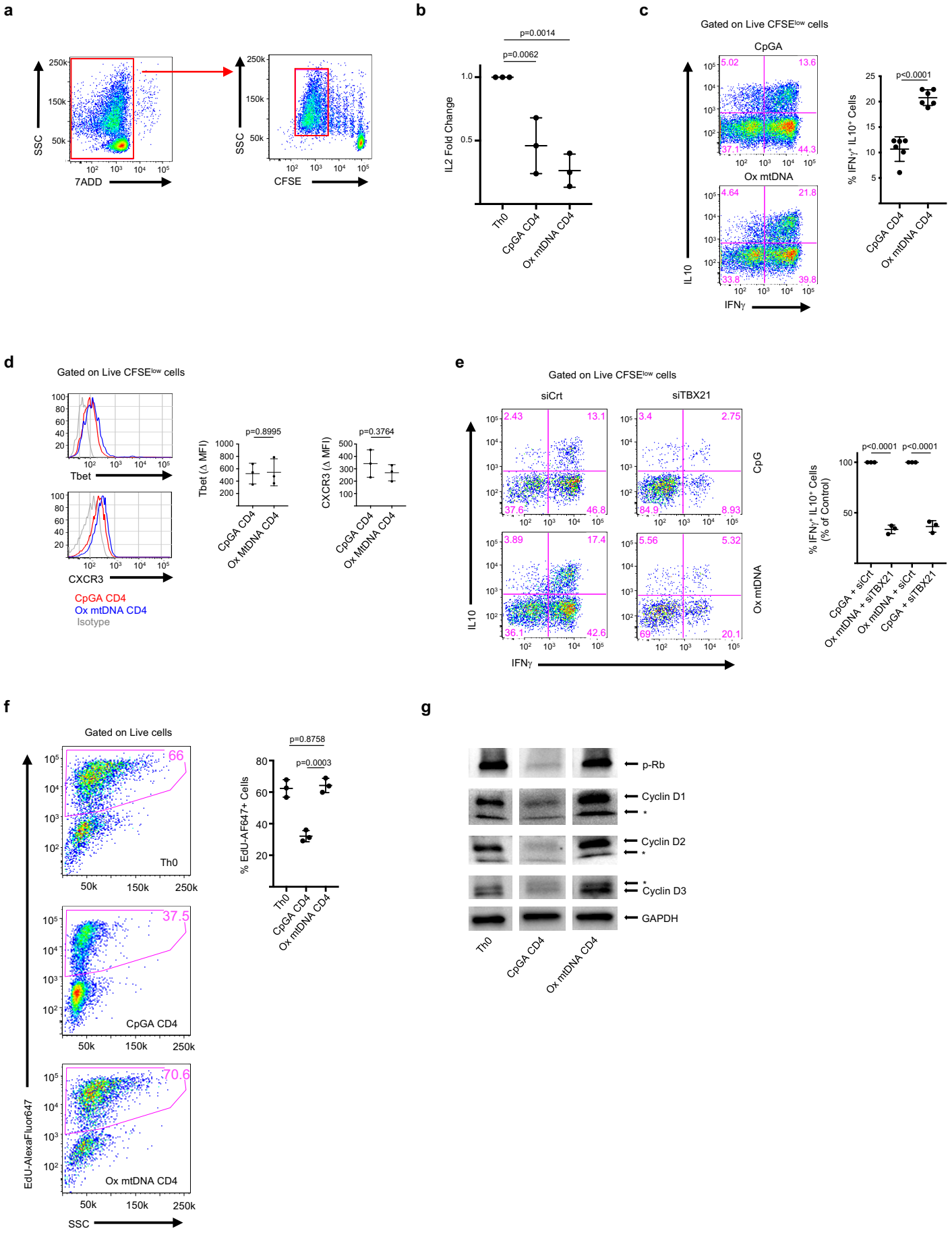

Supplementary Figure 2 | Ox mtDNA activated-pDCs generate proliferative IFNγ$^+$ IL10$^+$ CD4$^+$ T cells. a, Flow cytometry gating strategy to isolate activated (CFSE^{low}) CD4$^+$ T cells from pDC-naïve CD4$^+$ T cell co-cultures. This experiment was repeated ten times with similar results. **b,** QPCR-based detection of *IL2* gene expression, relative to Th0, in CpGA and Ox mtDNA CD4$^+$ T cells (n=3 independent experiments). **c,** Intracellular cytokine staining of CpGA or Ox mtDNA CD4$^+$ T cells upon reactivation with PMA/Ionomycin (n=5 independent experiments). Representative flow cytometry plots are also shown. **d,** T-bet and CXCR3 expression in IFNγ$^+$ IL10$^+$ CD4$^+$ T cells (n=3 independent experiments). Representative flow cytometry histograms are shown on the left. **e,** Intracellular cytokine staining of CD4$^+$ T cells generated in the presence of control (Crt) or *TBX21* small interfering siRNA (n=3 independent experiments). Representative flow cytometry plots are shown on the left. **f-g,** Proliferation (**f**; n=3 independent experiments) and representative immunoblot analysis (**g**; this experiment repeated three times with similar results) of Th0, CpGA or Ox mtDNA CD4$^+$ T cells upon reactivation with CD3/CD28. p-Rb; phosphorylated Retinoblastoma protein. * indicates non-specific band or alternative isoform. Shown are mean ± s.e.m.; statistical analysis by nonparametric one-way ANOVA (**b, f**) and two-tailed nonparametric unpaired *t*-test at 95% CI (**c-e**).

Supplementary Figure 3

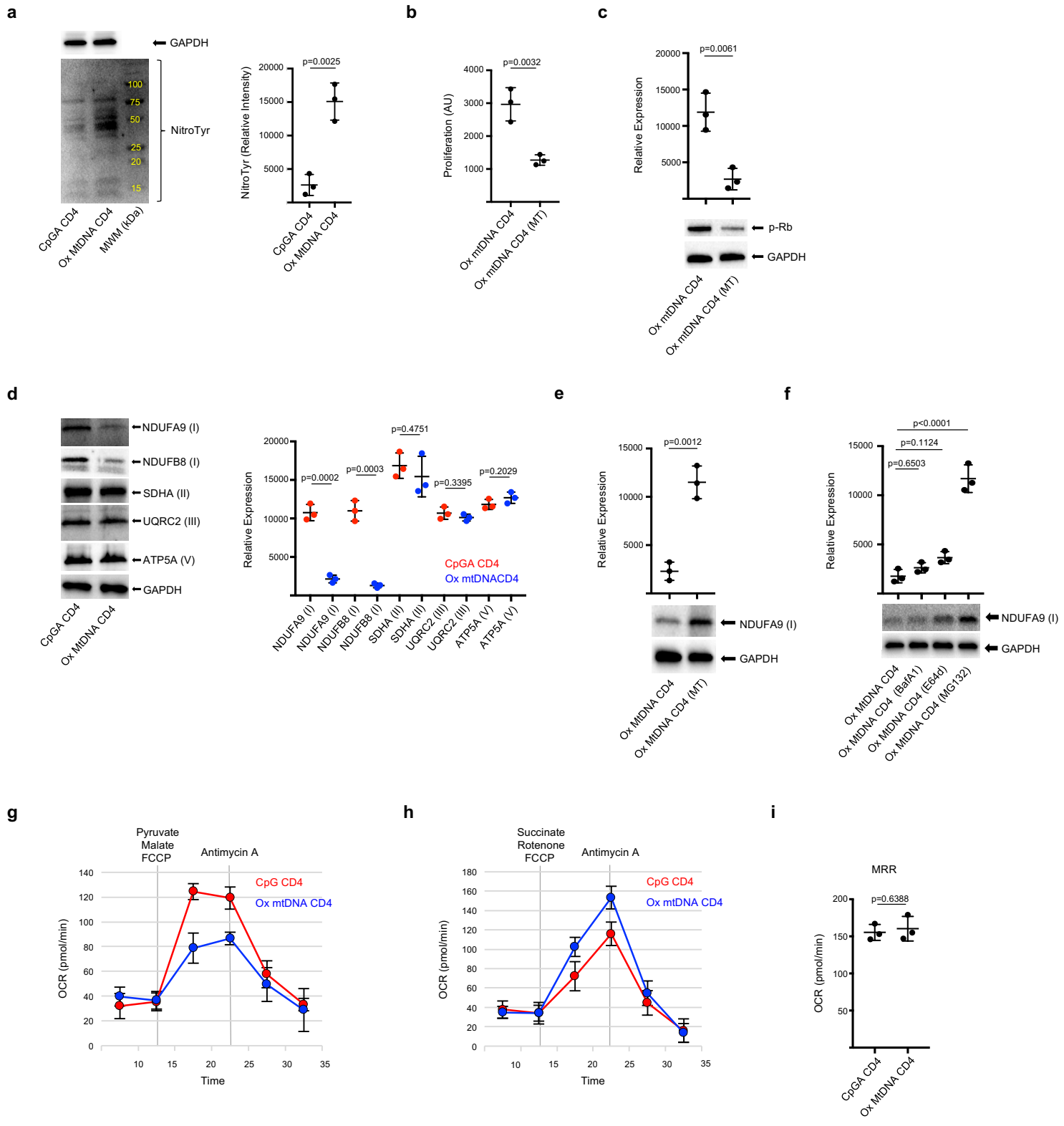

Supplementary Figure 3 | Ox mtDNA $CD4^+$ T cells accumulate mtROS and succinate. a, Representative Immunoblot (left) and relative quantification (right) of Nytrotyrosine levels in CpGA or Ox mtDNA $CD4^+$ T cells (n=3 independent experiments). **b,** Proliferation of Ox mtDNA $CD4^+$ T cells generated in the absence or presence of MitoTempo (MT; n=3 independent experiments). **c,** Immunoblot analysis of p-Rb in Ox mtDNA $CD4^+$ T cells generated in the absence or presence of MT. Relative quantification is also shown (n=3 independent experiments). **d,** Representative Immunoblot (left) and relative quantification (right) of mitochondrial respiratory chain subunits in CpGA or Ox mtDNA $CD4^+$ T cells (n=3 independent experiments). **e,** Immunoblot analysis of NDUFA9 (mitochondrial respiratory complex I subunit) in Ox mtDNA $CD4^+$ T cells generated in the presence of MT. Relative quantification is also shown (n=3 independent experiments). **f,** Immunoblot analysis of NDUFA9 in Ox mtDNA $CD4^+$ T cells treated with Bafilomycin A1 (BafA1), E64d or MG132. Relative quantification is also shown (n=3 independent experiments). **g,** Complex I activity was assessed by measuring the oxygen consumption rates (OCR) in response to the complex I substrate pyruvate. The complex II inhibitor malate was added togheter with pyruvate to block complex II-mediated respiration (n=3 independent experiments). **h,** Complex II activity was assessed by measuring the OCR in response to the complex II substrate succinate. The complex I inhibitor rotenone was added togheter with succinate to block complex I-mediated respiration (n=3 independent experiments). **i,** Maximal respiration rate (MRR) of CpGA and Ox mtDNA $CD4^+$ T cells (n=3 independent experiments). Shown are mean ± s.e.m.; statistical analysis by nonparametric one-way ANOVA (**f**) and two-tailed nonparametric unpaired *t*-test at 95% CI (**a-e; i**).

Supplementary Figure 4

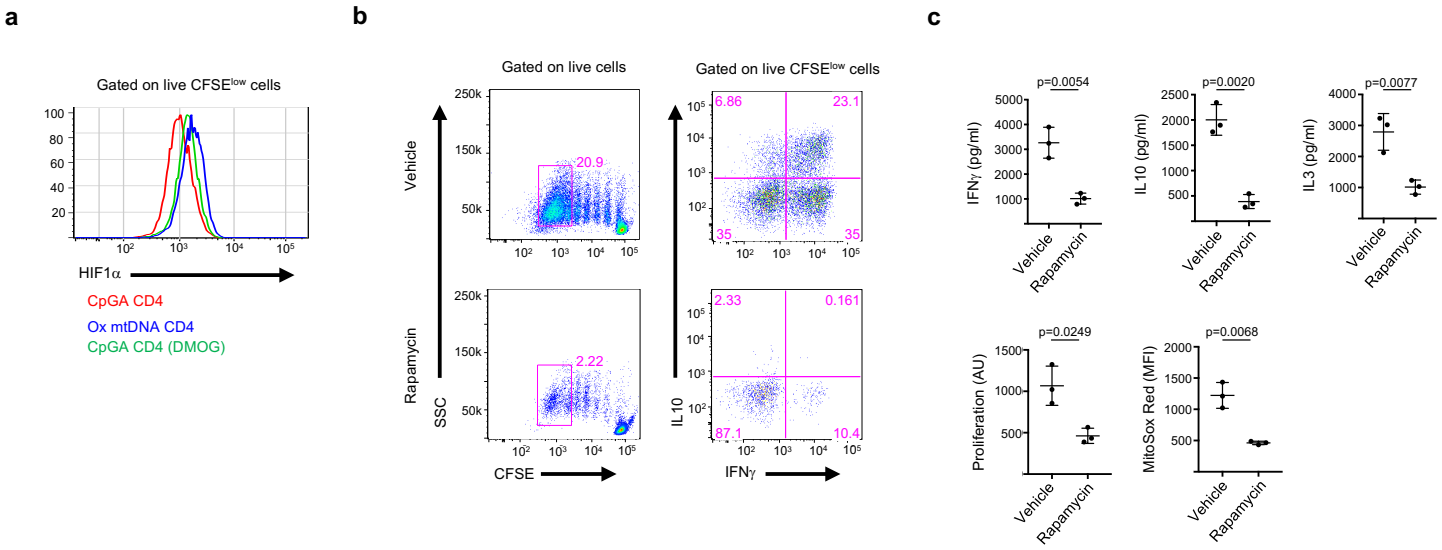

Supplementary Figure 4 | mTOR activation in Ox mtDNA CD4$^+$ T cells. a, Representative flow cytometry histogram of HIF1α intracellular levels. Dimethyloxalylglycine (DMOG). This experiment was repeated three times with similar results. **b,** Proliferation (left) and intracellular cytokine staining (right) of naïve CD4$^+$ T cells co-cultured with Ox mtDNA-activated pDCs in the presence or absence of rapamycin (100 nM). This experiment was repeated three times with similar results. **c,** Cytokine profile, proliferation and mtROS levels in Ox mtDNA CD4$^+$ T cells restimulated with anti-CD3/CD28 in the presence or absence of 100 nM of rapamycin (n=3 independent experiments). Shown are mean ± s.e.m.; statistical analysis by two-tailed nonparametric unpaired *t*-test at 95% CI.

Supplementary Figure 5

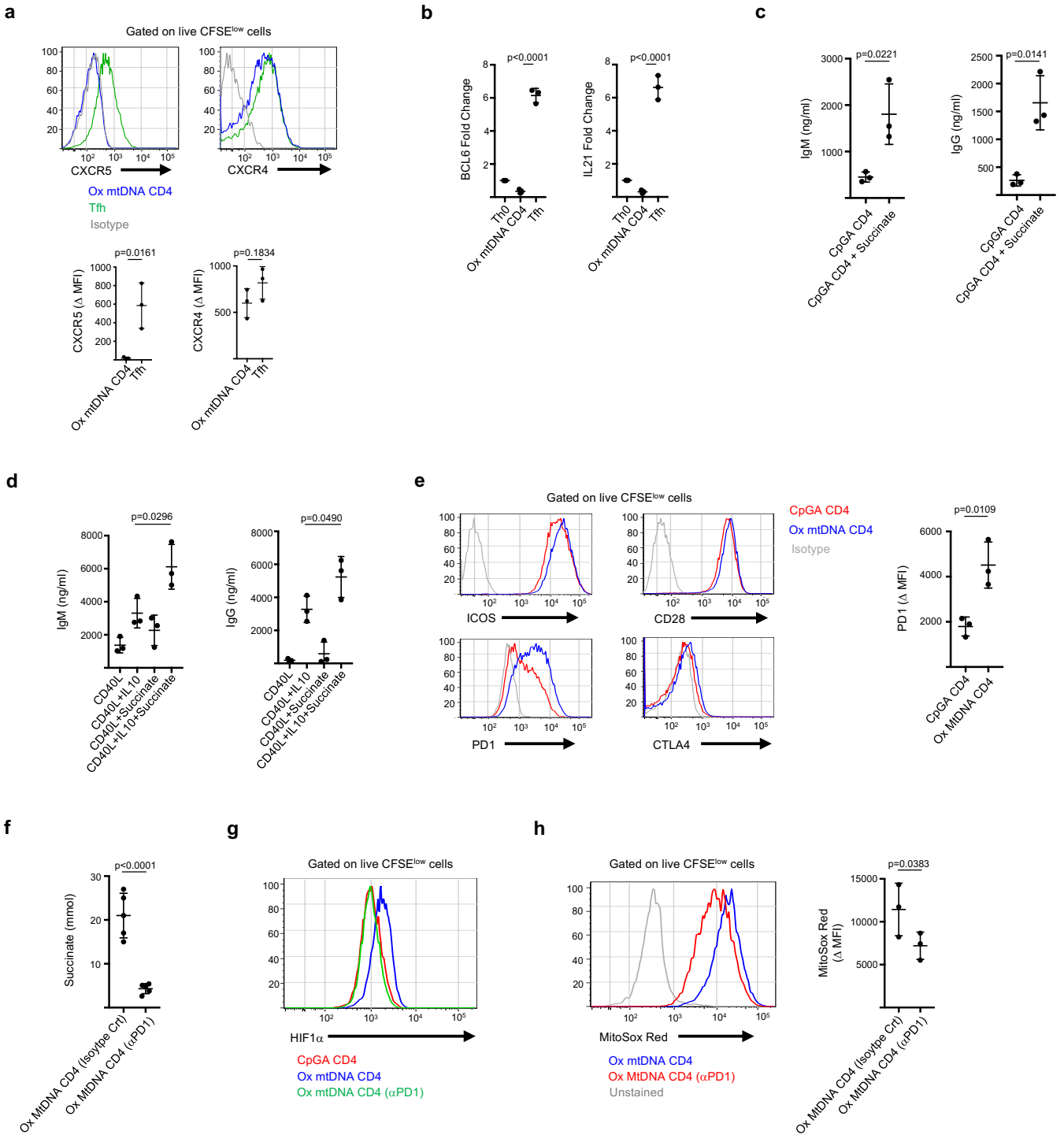

Supplementary Figure 5 | Ox mtDNA CD4$^+$ T cells accumulate mtROS and succinate in a PD1 dependent manner. a, Surface levels of CXCR5 and CXCR4 in CpGA and Ox mtDNA CD4$^+$ T cells (n=3 independent experiments). Representative flow cytometry histogram is also shown. **b,** QPCR-based detection of *BLC6* and *IL21* gene expression, relative to Th0, in Tfh or Ox mtDNA CD4$^+$ T cells (n=3 independent experiments). **c,** IgM and IgG levels in the supernatants from CpGA CD4$^+$ T cell and naïve B cell co-cultures upon succinate supplementation (n=3 independent experiments). **d,** IgM and IgG levels in the supernatants from CD40L-activated naïve B cells (n=3 independent experiments). **e,** Surface levels of ICOS, CD28, PD1, and CTLA4 on CpGA or Ox mtDNA CD4$^+$ T cells (n=3 independent experiments). **f,** Succinate levels in Ox mtDNA CD4$^+$ T cells generated in the presence of anti-PD1 antibody (n=5 independent experiments). **g,** Representative flow cytometry histogram of HIF1α intracellular levels. This experiment was repeated three times with similar results. **h,** MtROS levels, measured by MitoSOX Red, upon re-stimulation through CD3/CD28 (n=3 independent experiments). Shown are mean ± s.e.m.; statistical analysis by two-tailed nonparametric unpaired *t*-test at 95% CI (**a-c; e-h**) and nonparametric one-way ANOVA (**d**).

Supplementary Figure 6

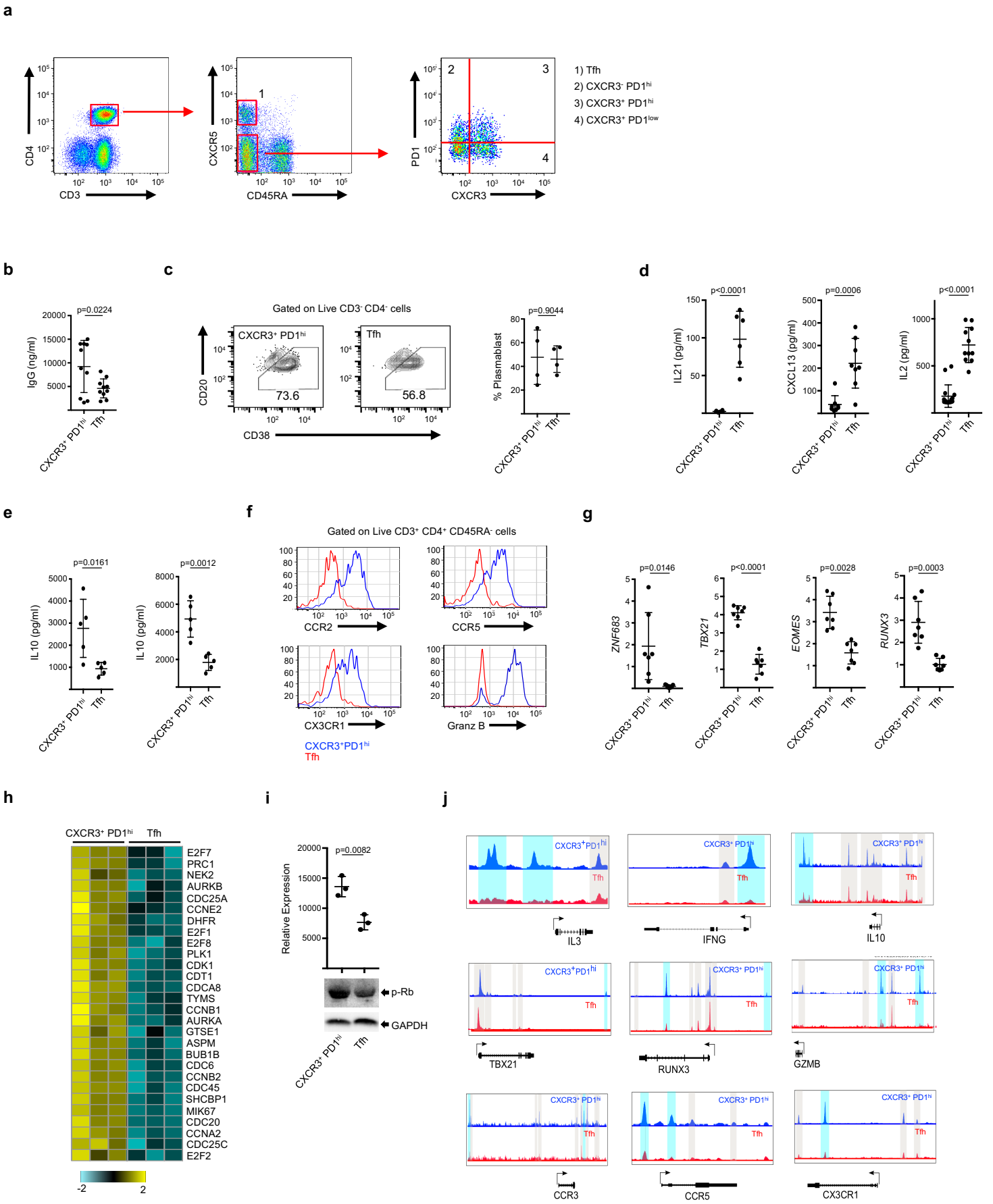

Supplementary Figure 6 | Memory CXCR5$^-$ CXCR3$^+$ PD1^{hi} CD4$^+$ T cells represent the blood counterpart of Ox mtDNA CD4$^+$ T cells. a, Flow cytometry gating strategy to isolate CXCR3$^-$ PD1^{hi} CD4$^+$ T cells, CXCR3$^+$ PD1^{hi} CD4$^+$ T cells, CXCR3$^+$ PD1^{low} CD4$^+$ T cells or Tfh cells from SLE blood. This experiment was repeated ten times with similar results. **b-c,** IgG levels (**b,** n=10 independent experiments) and CD20/CD38 expression (**c,** n=4 independent experiments) on memory B cells co-cultured with CXCR3$^+$ PD1^{hi} CD4$^+$ T cells or Tfh cells. **d,** IL21 (n=6), CXCL13 (n=8 independent experiments) and IL2 (n=11 independent experiments) levels in the supernatants of CXCR3$^+$ PD1^{hi} CD4$^+$ T cells and Tfh cells upon reactivation with CD3/CD28 for 24 h. **e,** IL10 levels in the supernatants from CXCR3$^+$ PD1^{hi} CD4$^+$ T cell or Tfh cell and naïve (left) or memory (right) B cell co-cultures (n=5 independent experiments). **f,** CCR2, CCR5, CX3CR1 and Granzyme B expression levels in CXCR3$^+$ PD1^{hi} CD4$^+$ T cells and Tfh cells. This experiment was repeated three times with similar results. **g,** Transcription factor expression in CXCR3$^+$ PD1^{hi} CD4$^+$ T cells and Tfh cells (n=7 independent experiments). **h,** Differentially expressed cell cycle gene signature, selected accordingly to DAVID analysis, in CXCR3$^+$ PD1^{hi} CD4$^+$ T cells and Tfh cells (n=3 independent experiments). **i,** Immunoblot analysis of p-Rb in CXCR3$^+$ PD1^{hi} CD4$^+$ T cells and Tfh cells. Relative quantification is also shown (n=3 independent experiments). **j,** Normalized ATAC-seq signal profiles across IL3, IFNγ, IL10, TBX21, RUNX3, GZMB, CCR3, CCR5 and CX3CR1 loci. Peaks detected in both populations (grey) and opening only in CXCR3$^+$ PD1^{hi} CD4$^+$ T cells (light blue) are highlighted. This experiment was repeated two times with similar results. Shown are mean ± s.e.m.; statistical analysis by two-tailed nonparametric unpaired *t*-test at 95% CI.

Supplementary Figure 7

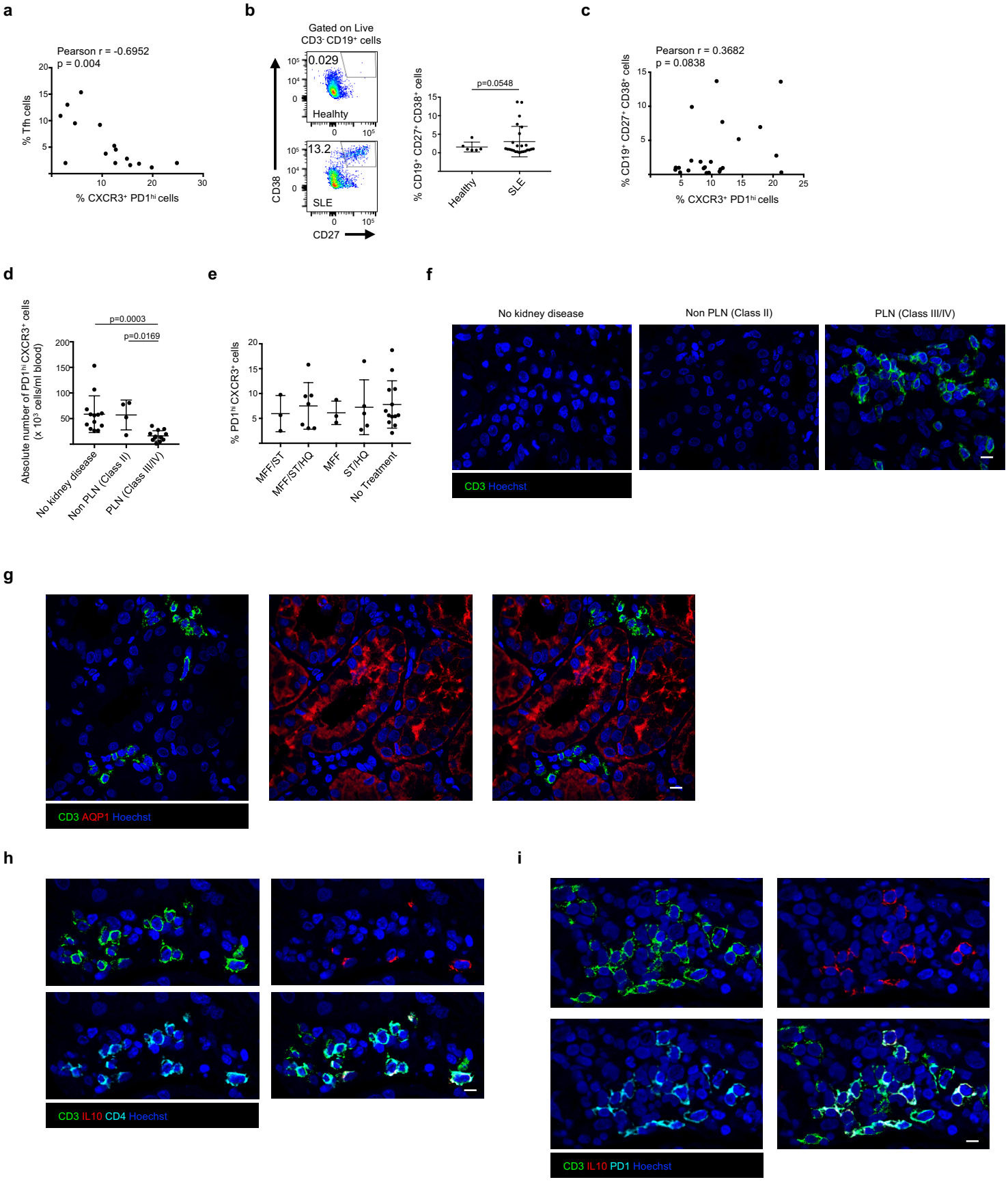

Supplementary Figure 7 | IL10$^+$ IFNγ$^+$ ROS$^+$ PD1$^+$ CD4$^+$ T cells accumulate in PLN lesions. a, Pearson correlation analysis between the frequencies of SLE blood CXCR3$^+$ PD1^{hi} CD4$^+$ T cells and CXCR5$^+$ CD4$^+$ T cells (Tfh) (n=15 biologically independent samples). **b,** Representative flow cytometry dot plots (left) and frequency of plasmablasts among CD3$^-$ CD19$^+$ cells (right) in the blood of healthy donors (n=6 biologically independent samples) or SLE patients (n=25 biologically independent samples). **c,** Pearson correlation analysis between the frequencies of blood CXCR3$^+$ PD1^{hi} CD4$^+$ T cells and plasmablasts (n=23 biologically independent samples). **d,** Absolute numbers of CXCR3$^+$ PD1^{hi} CD4$^+$ T cells in blood of SLE patients with nephritis Class II (n=4 biologically independent samples), Class III/IV (PLN; n=12 biologically independent samples) or without kidney disease (n=13 biologically independent samples). **e,** Frequency of blood CXCR3$^+$ PD1^{hi} CD4$^+$ T cells in patients according to treatment combinations of mycophenolate mofetil (MFF), oral corticosteroids (ST), hydroxychloroquine (HQ) or no treatment (n=31 biologically independent samples). **f,** Representative immunofluorescence microscopy of CD3 staining in patients with either no kidney disease (n=6 biologically independent samples), non PLN (n=4 biologically independent samples; class II) or PLN (n=17 biologically independent samples; class III/IV). Representative dHPF are shown. **g,** Representative immunofluorescence microscopy of CD3 and the proximal tubular marker Aquaporin1 (ACQ1) staining in a class IV LN section. One dHPF representative of four is shown. **h,** Representative immunofluorescence microscopy of CD3, CD4 and IL10 staining in a class IV LN section. One dHPF representative of four is shown. **i,** Representative immunofluorescence microscopy of CD3, PD1 and IL10 staining in a class IV LN section. One dHPF representative of four is shown. Scale bar = 10 μm. Shown are mean ± s.e.m.; statistical analysis by two-tailed nonparametric unpaired *t*-test at 95% CI (Welch's correction).

Supplementary Figure 8

a

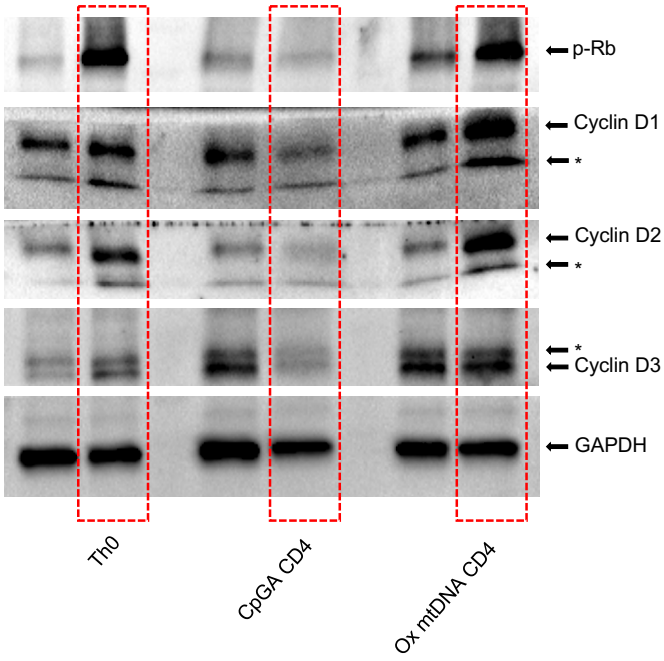

Supplementary Figure 8 | Uncropped western blot of Supplementary Figure 2g. * denotes non specific bands and/or different isoforms.